MICROSTRUCTURAL IMPROVEMENTS OF SAC ALLOYS WITH BI ADDITIONS DURING ACCELERATED THERMAL CYCLING

Eva Kosiba[1], Polina Snugovsky[2], John McMahon[2], Doug Perovic[3]
[1]Zebra Technologies, [2]Celestica, [3]University of Toronto
Mississauga ON, Canada

ABSTRACT
Tin based Pb-free solders continue to present challenges in high reliability applications, particularly when exposed to accelerated thermal conditions. Bi as an alloying element has been found to have beneficial properties, both by reducing the overall process temperature and through intrinsic material characteristics. This paper explores the microstructural evolution of three Pb-free solders; two have a near-eutectic composition in a quaternary system, while a third has a composition along the eutectic valley of a ternary compound. The properties and microstructures of each are compared to SAC305. Reduced amount of Ag, including one alloy with no Ag, are also examined. Changes to the bulk microstructure and the interfacial IMC between time of solidification and exposure to accelerated thermal cycling are explored and compared with reliability data. Two thermal cycling conditions are considered, 0 to 100°C and -55 to 125°C.

Key words: Lower Melt solder, Bi-containing solder

ACCELERATED TESTING FOR RELIABILITY ANALYSIS

Reliability can be defined as the probability of a product to meet specifications over a given time period while subjected to determined environmental conditions.[1] The reliability of any electronic assembly depends on the reliability of each individual element. An assembly is likely to fail due to component failure in the short term and due to solder attach failure in the long term.[2] The solder attach, which include the solder joint and the material to which it adheres, particularly in the case of surface mount devices, presents a complicated situation in that it acts as both the electrical contact as well as the mechanical attachment.[3] In field operation, a solder attach will experience loading conditions in the form of: (i) mechanical load, (ii) vibration, (iii) thermal shock and (iv) differential thermal expansion. The accumulated damage caused by one or more of these stress conditions will eventually lead to wear-out failure. Therefore, determination of the useful life of an electronic product is contingent upon the understanding of the failure rate of the surface mount solder attach.

Accelerated testing is used to obtain more information than would be practical, or even possible, under normal field conditions where years may pass before a sufficient number of failures occur to determine the reliability of a product. Accelerated testing is also essential in determining the effects of changes to product design through its design cycle. Accelerated conditions may include a test environment in which conditions are more severe than that experienced during normal equipment use or by increasing the frequency in which a condition is applied to a product. In both cases, care should be taken to avoid the introduction of failure mechanisms, which would not be encountered in field operation of a product.4 If failure mechanisms are maintained, the accelerated data can be used to extrapolate the expected failure rates in field conditions.[2]

Of the four loading conditions described above, thermomechanical fatigue resulting from cyclic differential thermal expansion is the primary failure mechanism of surface mount solder joints and the focus of this chapter.[3,5] This form of fatigue is the combination of plastic and creep deformation which occurs as a solder attach is exposed to cyclical heating and cooling through powering on and off, as well as exposure to environmental conditions. Accelerated Thermal Cycling (ATC) is used to test the response of a product to rapidly repeating changes in temperature to a level higher than normally experienced by a product in field conditions. In this case, the applied cyclical stress is in the form of differential thermal expansion and contraction between the various materials within a circuit board. These differences are defined by the coefficient of thermal expansion (CTE) of the differing materials that make up the system. In a circuit board, there are two levels of recognized differential thermal expansion:

1. Global: thermal expansion mismatch between components and substrate, as illustrated in Figure 1.
2. Local: thermal expansion mismatch between solder and material to which it is bonded[6]

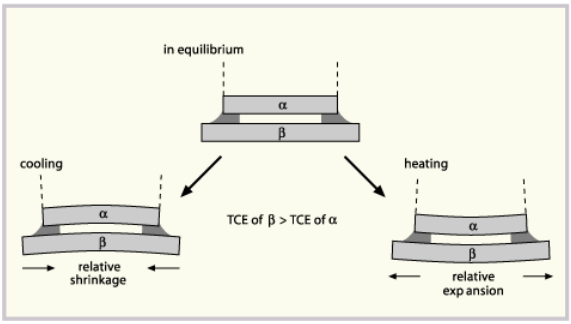

Figure 1: Representation of stress generated in circuit due to CTE mismatch[7]

Stress-strain hysterisis loops, such as the one illustrated in Figure 2, are often used to describe the cumulative stress history experienced by a solder attach during ATC. As the temperature increases, the differential expansion of the various materials results in the initial applied stress, which leads to plastic deformation. During the hot dwell (or hold) period, which generates stresses lower than the yield strength of the solder, creep and stress relaxation within the solder material occur. During accelerated testing, there may or may not be enough time allotted for full stress relaxation as would likely exist in field conditions. Stress is then applied in the opposite direction – the stress axis representing an absolute value – during the cold cycle. As the cycles are repeated, the solder joint fails due to low-cycle fatigue and can be described by the Coffin-Manson relationship given in Equation 1:

$$\overline{N}_f = C_1(\Delta\gamma_p)^{1/m} \qquad \mathbf{1}$$

where $\overline{N}_f$ is the average number of cycles to failure, C_1 and m are material constants.[8] Greater temperature fluctuations or greater differences in CTE mismatch will result in higher values of plastic shear strain ($\Delta\gamma_p$). This value will also be impacted by component geometry. For example leaded components will result in lower shear plastic strain than leadless components. Ramp rate and dwell time, at the temperature extremes, will also impact the shape of the hysteresis loop and the strain level. The Coffin-Manson model assumes that plastic strain is the main deformation mechanism. This simplified model has since been revised to include the more dominant creep effect, as well as cyclical parameters. These models are presented in IPC-SM-785 and take into account such factors as component and solder fillet geometry, potential cyclic fatigue damage at complete stress relaxation, and fatigue ductility coefficients. These models are also presented with numerous caveats indicating which conditions are required for each model and what limitations may exist.[2] Modeling of complex creep-fatigue in solder attach, particularly for new solder alloys, is a continuing field of research.

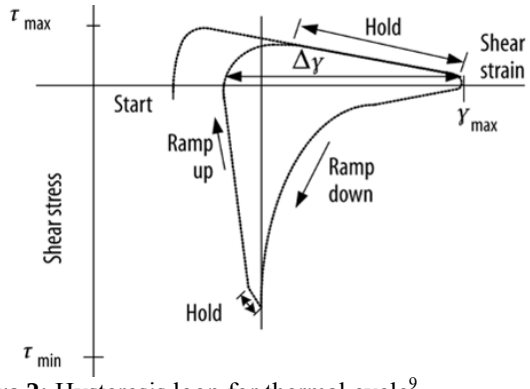

Figure 2: Hysteresis loop for thermal cycle[9]

In order to relate the results of ATC testing, or any Accelerated Life Testing (ALT), to life condition, data from at least two conditions need to be used to establish a trend line in order to extrapolate to field condition. Low-level and a high-level acceleration condition should be chosen. Three or more conditions would allow for determination of non-linear relationships. Low-level acceleration should produce a mean time-to-failure (MTTF) of about 10-20 times shorter than the actual field life. High-level acceleration should produce a MTTF of approximately 100-500 times shorter than actual field life.[2] Acceleration Factors (AF) are then calculated as the ratio between the two conditions and then extrapolated from the chosen conditions to field conditions.

ATC qualification test conditions for various applications have been determined and compiled in specification IPC-9701A[6]. These tests have been devised as minimum criteria for accelerated testing for qualification purposes. While Appendix 1 of this specification does provide guidance and examples for determining AF, it is not necessary to determine these for every test. Rather, the minimum requirements per industry have been established. This specification also states at least 32 samples per condition should be tested and the test should run for the required duration or at least until 63.2% failure in order to characterize the failure distribution. Tests that are stopped at the end of the required Number of Thermal Cycle (NTC) level with insufficient (or no) failures will be characterized by failure analysis (FA) alone. FA is to be performed on a minimum of three randomly chosen samples. Table 1 provides a summary of the test conditions laid out in this standard and Table 2 provides some examples of worst-case scenarios for various products in field conditions.

Table 1: Sample of temperature cycling requirements Table 4-1 in IPC-9701A[6]

Test Condition	Mandated Condition	Test Duration	Low Temp. Dwell	High Temp. Dwell	Temp. Ramp Rate
TC1	0°C - 100°C	NTC-E 6,000 cycles (preferred for TC1)	10 minutes (+0°C/-5°C)	10 minutes (+5°C/-0°C)	≤20°C/minute
TC4	-55°C - 125°C	NTC-C 1,000 cycles (preferred for TC4)			

Table 2: Worst case use environments of SMT[6]

Application	T_{min} (°C)	T_{max} (°C)	ΔT (°C)	Cycles/ year	Typical service life (years)	Acceptable failure risk (%)
Consumer	0	60	35	365	1-3	1
Military Aircraft a) b) c)	-55	125	 40 60 80	 100 100 65	10-20	0.01

Note in Table 2, ΔT is not simply the difference between T_{max} and T_{min} representing the absolute maximum and minimum temperatures experienced in the given environment, but rather the expected worse-case scenarios which occur in a given service condition.[2]

Solder in ATC testing has been shown to fail according to a creep-fatigue model resulting from the applied thermomechanical fatigue stresses. The mechanical properties of solder are temperature dependent and therefore change continuously over the course of a fatigue cycle, both in the bulk microstructure of the solder as well as in the IMC layer formed between the solder and the Cu substrate. There are also cumulative effects of repeated cycles.[10] The total strain (ε_T) can be expressed by Equation 2 where ε_e and ε_p are the elastic and plastic strains respectively and ε_c represents creep strain.

$$\varepsilon_T = \varepsilon_e + \varepsilon_p + \varepsilon_c \qquad 2$$

During the high temperature dwell period of the thermal cycle, creep and stress relaxation are the dominant strain evolution mechanisms. During ramp up and down, plastic and elastic strain deformations are dominant unless this transition is slow enough to allow for full stress relaxation, which is not typically the case in accelerated testing. It is the repeated plastic and elastic strain which constitutes fatigue fracture.

MICROSTRUCTURAL EVOLUTION

Changes to Bulk Solder:

Notably, many of the tests and models described above have been developed for SnPb solders, which have been tested over decades. It has been shown that the microstructural response to creep and fatigue behavior of Sn based SAC alloys is very different than that of SnPb.[11] Therefore, it is possible the models and even the applicable test conditions need to be updated. In SnPb solder joints, the initial response to applied thermomechanical stress is grain coarsening in an attempt to reduce the internal energy in the smaller grains. Both the applied shear strain which results from CTE mismatch and the elevated temperature aid in grain coarsening. In eutectic SnPb, the Sn rich regions and Pb regions will coalesce into larger islands. During coarsening, it should be noted that the IMC attach layer also thickens – a Cu_3Sn region may form between the Cu substrate and the Cu_6Sn_5. Immediately adjacent to the IMC a layer of Pb-rich phase will form as the local Sn has been consumed in the IMC growth process. Pb also tends to pool around the grain boundaries of the Sn rich phase. Grain coarsening is accomplished via grain boundary sliding and grain boundary diffusion-induced migration.[5] Microvoids begin to appear along grain or interphase. Microvoids continue to propagate along grain boundaries or other interfaces until they connect to form microcracks and eventually catastrophic macro level cracks. Figure 3 illustrates a typical SnPb solder attach a) before any accelerated testing and b) after 3000 cycles of harsh ATC. These images, taken at the same magnification, illustrate the degree of grain coarsening, IMC growth and phase coalescence that occurs during repeated stress cycles. While this joint did not fail catastrophically after 3000 cycles, a large crack is propagating through the bulk solder along a Pb-rich region and, if testing had continued, would have lead to a full electrical and mechanical fail.

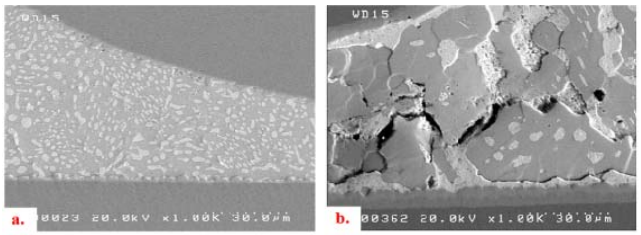

Figure 3: SnPb solder a) before testing and b) after 3000 cycles -55°C to 125°C[12]

The microstructure of solder attach formed with SAC type alloys are found to behave differently from that of eutectic SnPb. The solders in this study are made up of up to 98% Sn with small amounts of Ag and Cu present as intermetallics. The βSn matrix, as well as the Ag_3Sn and Cu_6Sn_5 precipitates all influence the creep response of the solder attach. As the strain increases, an initial coarsening of the IMC particles occurs. Recrystallization of the Sn grains takes place in the area of high strain, usually close to the bulk solder interface with the attach IMCs. The grain boundaries formed between these new grains, as well as some large precipitates, provide sites along which voids can form (at the triple points) and fractures can easily propagate.[10,13] Additionally, it is during the hot dwell cycle that the brittle IMC attach layer may grow.[7]

Figure 4 shows a solder attach made up of SAC305 a) before testing and b) after 3000 cycles of harsh testing. From Figure 4a) we can see the dendritic arms of the βSn appear relatively small and evenly spaced with small dispersiods of Ag_3Sn in the interdendritic spacing. After ATC, the Ag_3Sn particles appear to have coalesced into fewer, larger particles. Additionally, the IMC layers formed between the lead and solder as well as between the solder and copper pad have increased in size and appear to have two phases, Cu_3Sn and Cu_6Sn5 as seen in Figure 4b). A Cu_3Sn layer was not detectable at zero time. Finally, the dendritic structure does not appear to be well defined after thermal cycling. Polarized light or electron backscatter diffraction (EBSD) is needed to properly view the grain structure. Figure 5 shows an example of a BGA solder joint that failed during thermal cycling; recrystallized grains appear in the region where high shear strength is experienced, and where the final crack propagated. Using EBSD, it has been proposed that this recrystallization occurs ahead of the propagating crack.[10] Fractures can easily propagate along the regions created under creep conditions, notably between grain boundaries and along the bulk solder/IMC interface.

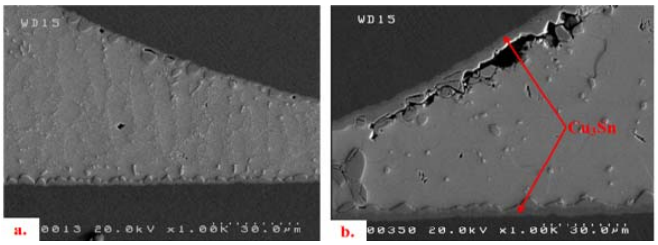

Figure 4: SAC305 solder a) before testing and b) after 3000 cycles -55°C to 125°C[12]

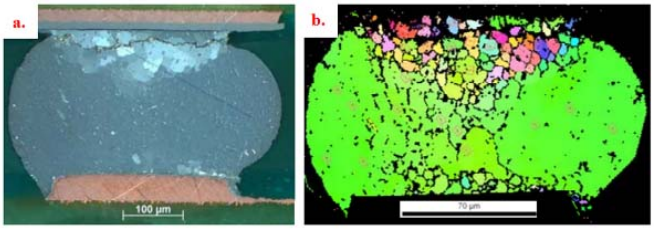

Figure 5: SAC305 after ATC shown with a)polarized light and b)EBSD mapping [13]

Changes to Interfacial IMC during Accelerated Thermal Cycling:

A good interfacial IMC layer is required for a properly formed solder joint, as it provides the mechanical, electrical and thermal connection between the bulk solder and the Cu substrate. This layer, however tends to be brittle and if a very thick layer forms or develops, it may become a reliability concern. Interface layers also tend to be preferential sites for crack formation and propagation. Additionally, the IMC layer in solder joints may be a reliability concern because it consumes Cu from the substrate, Cu being the dominant diffusing species.[14] The consumption of Cu may result in a weakened Cu pad.

Cu_3Sn was not detected upon initial solidification; it forms as a result of solid-state reaction during thermal aging at temperatures above 60°C.[17] The Cu_3Sn growth occurs between the Cu_6Sn_5 and the Cu substrate and is governed by the availability of Cu from the substrate and Sn either from the already present Cu_6Sn_5 as described in equation 3 or Sn from the bulk solder diffusing through the Cu_6Sn_5 substrate as described in equation 4. The initial formation of Cu_6Sn_5, and its continued growth are dependent on Sn from the bulk solder and Cu from the substrate. The Cu is either present during the initial solidification reaction, or diffuses through the Cu_3Sn layer. Both are described by equation 5.[15]

$$Cu_6Sn_5 + 9Cu \rightarrow 5Cu_3Sn \quad \textbf{3}$$

$$3Cu + Sn \rightarrow Cu_3Sn \quad \textbf{4}$$

$$6Cu + 5Sn \rightarrow Cu_6Sn_5 \quad \textbf{5}$$

The Cu_3Sn layer is of concern for three reasons: it is a brittle layer more so than Cu_6Sn_5 or bulk solder, it is associated with large volume shrinkage, and the growth of a Cu_3Sn layer next to Cu is often accompanied by Kirkendall voids along the interface of the two phases.[16] These small voids may form a weak interface.

Both Ag and Cu additives to the solder have been found to be beneficial in suppressing the growth of the Cu_3Sn layer.[17] Ag does not participate in the interfacial IMC layer at all and can therefore only act as an influence by retarding the diffusivity of Sn through the bulk solder towards the IMC layer. Other alloying elements (e.g. Ni, Zn) have also been found to retard the growth of Cu_3Sn and in some instances Cu_6Sn_5. In these cases, trace amounts of the element are found in, or at the interface of the IMC layer and therefore are thought to participate directly in the reaction or provide a diffusion barrier between the layers.[18]

The change in thickness of the intermetallic layers can be described by the Arrhenius equation (6) where x is the thickness, x_0 is the initial thickness in m, t is time in s, T is temperature in K, R is the universal gas constant (8.314 kJ/mol K) and A, Q and n are material constants. [20]

$$x - x_0 = At^n \exp(-Q/RT) \quad \textbf{6}$$

Effects of Bi:

Bi as an alloying element is expected to have an overall influence on the reliability of a solder joint in two ways. The first is the reduced process temperature due to the addition of Bi, which may result in a reduced thickness of the interfacial IMC layer as well as reducing some of the deleterious effects of high temperature on both board material and components.[19]

The second involves modification of the bulk solder microstructure. βSn phase is considered to have most potential for modification with alloying as it makes up most of the volume within a SAC solder joint. Alloys with Bi have been explored as a means to improve thermomechanical properties through solid solution strengthening and precipitate hardening.[20] In a previous study, for example, after 3000 cycles harsh environment ATC (-55°C to 125°C), Bi which was previously present in solid solution with βSn precipitated out in an evenly distributed manner, reducing microstructural degradation.[12] Other studies have shown that Bi segregates at the grain boundaries, potentially reducing creep resistance.[21]

The influence of Bi on the formation of interfacial IMC layers has also been explored. It has been shown that Bi does not participate in the formation of either intermetallic compound layers (Cu_6Sn_5 or Cu_3Sn), but there is a higher concentration within the βSn close to the Cu_6Sn_5 suggesting that Bi is rejected from the βSn as Sn is contributed to the formation of Cu_6Sn_5.[22]

In this thesis, the behavior of Bi containing alloys is investigated. Also, the impact of reducing the amount of Ag in SAC-based solders is also examined.

EXPERIMENTAL SETUP

The work in this section forms a screening experiment in which the performance of selected alloys was evaluated during thermal cycling under two different conditions. The intention was to provide data for determining the suitability of these solders for more statistically relevant reliability testing, which is too costly to perform on all combinations of solder, board material and temperature conditions. These tests were performed in accordance with test conditions outlined in IPC-9701A[6] and IPC-SM-785[2]. The statistical requirements of these specifications were not adhered to due to limited resources.

ATC testing assumes that solder joints were properly formed and no wetting issues exist, which would result in infant mortality due to defective solder joints.[6] The quality of solder joints used in this study was demonstrated to be satisfactory. In addition to testing a statistically relevant number of samples, IPC-9701A states that the duration of testing would ideally generate at least 63.2% failures within that sample set in order to properly evaluate reliability and possibly determine acceleration factors. This specification states that if an insufficient number of failures, or no failures at all, are generated at the end of the number of thermal cycles (NTC) level, then failure analysis should be performed on a random selection of parts (a minimum of three per test variation) to verify that no failure occurred. This failure analysis can also be useful in determining whether or not any microstructural changes occurred during the testing. Finally, as this testing is intended to address solder joint reliability, only those failures determined to be the result of thermomechanical component/board interaction will be considered. Board level failures such as via cracks, delamination, will not be included in the data set for any solder joint reliability calculations.[6]

Materials:

Three Bi-containing alloys, Senju M42 containing 3%Bi and Sunrise and Sunflower each containing 7wt% Bi, with low or no Ag, were tested against SAC305. Two board materials were tested; a normal T_g material– one which is typically used for SnPb applications around 150°C, and a high T_g material– one which is now required for most Pb-free applications at around 170°C. Table 3 summarizes the combinations of solder and board material tested. The lower T_g board materials that had been previously used with SnPb solders had a lower elastic modulus and were less susceptible to pad cratering, delamination and warpage failures.

Table 3: Build matrix for ATC testing

Alloy	Composition	Board Material	Assembly Temperature
SAC305	Sn 3%Ag 0.5%Cu	High T_g (170°C)	240°C
Senju M42	Sn 2%Ag 0.75%Cu 3%Bi		224°C
Sunrise	Sn 1%Ag 0.7%Cu 7%Bi		222°C
Sunflower	Sn 0.7%Cu 7%Bi		226°C
SAC305	Sn 3%Ag 0.5%Cu	Normal T_g (150°C)	240°C
Senju M42	Sn 2%Ag 0.75%Cu 3%Bi		224°C
Sunrise	Sn 1%Ag 0.7%Cu 7%Bi		222°C
Sunflower	Sn 0.7%Cu 7%Bi		226°C

Test Vehicle:

The test vehicle shown in Figure 6 was selected for this work. It was designed to simulate a typical, medium complexity SMT assembly. It is an 8”x10” surface made up of 12 copper layers for a total thickness of 0.093” with an Organic Solderability Preservative (OSP) finish. This board is often used to test new, lead-free solders and other material parameters. LQFP176, PBGA256, CBGA64 and MLF20s were populated, two of each per board. The BGA components all had SAC305 ball alloy and all component groups were reflowed in an air environment. Figure 6 and

Table 4 shows the test vehicle and highlights the monitored components.

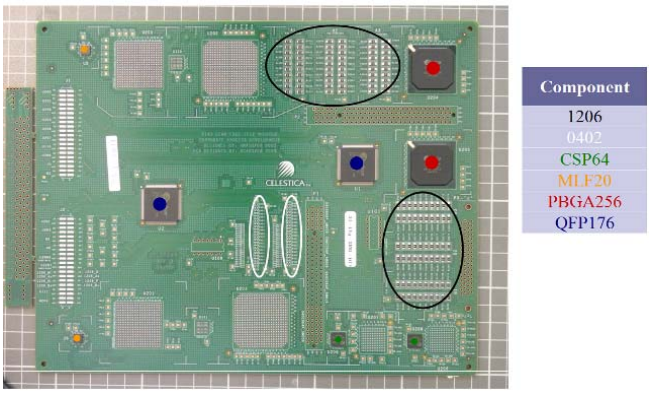

Figure 6: Test vehicle with monitored components

Table 4: Monitored components for ATC testing

Component	Reference Designator
1206	1206-A1
1206	1206-B1
0402	R400-R419
0402	R420-R439
CSP64	U208
CSP64	U209
MLF20	U5
MLF20	U6
PBGA256	U204
PBGA256	U205
QFP176	U1
QFP176	U2

Test Strategy:

All components were monitored using electrical data loggers; failures were defined as a 20% increase in nominal resistance over five consecutive scans. Failures were cut from the boards, and then the rest of the components were

returned to the chamber for further testing. Each of the two thermal profiles was allowed to run for a preset number of cycles.

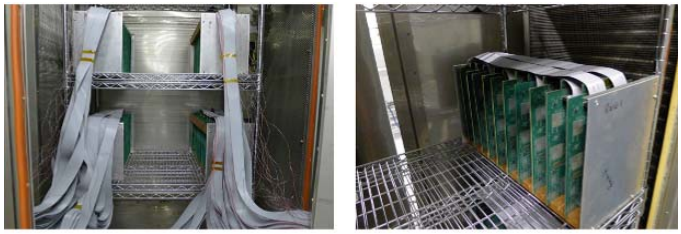

Figure 7: Card set up in thermal cycling chamber

0-100°C Thermal Cycling:
This portion of the testing was done in accordance with IPC-9701A Test Condition 1 (TC1) of 0°C (+0/-5°C) to 100°C (+5/-0°C) for Number of Thermal Cycles (NTC-E), which is preferred for TC1, of 6000 cycles. The boards under test, listed in Table 5 were set up in a chamber using a racking system which allowed for airflow around the boards (Figure 7). The final thermal cycle profile is shown in Figure 8.

Table 5: Test matrix for 0°C to 100°C ATC

Alloy	Composition	Board Material	# of Boards Tested
SAC305	Sn 3%Ag 0.5%Cu	High T_g (170°C)	4
		Normal T_g (150°C)	3
Senju M42	Sn 2%Ag 0.75%Cu 3%Bi	High T_g (170°C)	6
		Normal T_g (150°C)	5
Sunrise	Sn 1%Ag 0.7%Cu 7%Bi	High T_g (170°C)	5
		Normal T_g (150°C)	6
Sunflower	Sn 0.7%Cu 7%Bi	High T_g (170°C)	5
		Normal T_g (150°C)	5

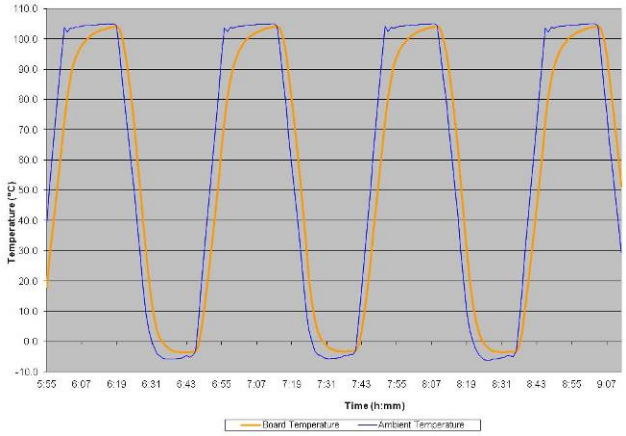

Figure 8: Chamber profile for 0°C to 100°C thermal cycling

Harsh Environment (-55°C to 125°C) Thermal Cycling:
This portion of testing was done in accordance with IPC-9701A Test Condition 1 (TC4) of -55°C (+0/-5°C) to 125°C (+5/-0°C) for NTC-C of 1000 cycles. Notably, the maximum temperature selected for the thermal cycle profile should be 25°C lower than the T_g of the board material.[6] In this case the Normal T_g board material is 150°C, while it is exactly 25°C lower than the T_g, does not allow for the 10°C leeway on the hot end of the cycle making the board material vulnerable to damage during testing. The boards under test are listed in Table 6. The final thermal cycle profile is shown in Figure 9.

Table 6: Test matrix for -50-125°C ATC

Alloy	Composition	Board Material	# of Boards Tested
SAC305	Sn 3%Ag 0.5%Cu	High T_g (170°C)	3
		Normal T_g (150°C)	3
Senju M42	Sn 2%Ag 0.75%Cu 3%Bi	High T_g (170°C)	5
		Normal T_g (150°C)	5
Sunrise	Sn 1%Ag 0.7%Cu 7%Bi	High T_g (170°C)	5
		Normal T_g (150°C)	6
Sunflower	Sn 0.7%Cu 7%Bi	High T_g (170°C)	5
		Normal T_g (150°C)	5

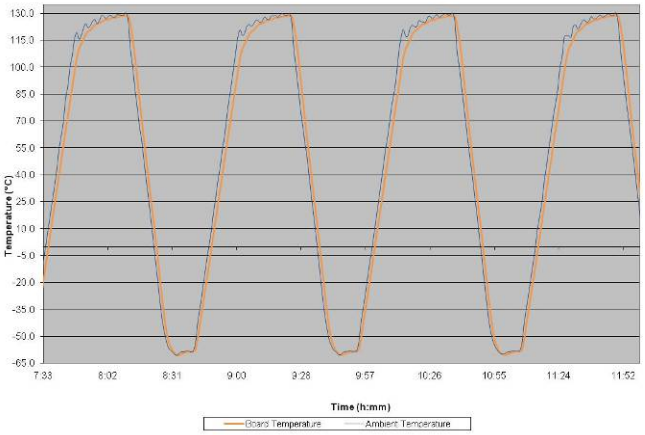

Figure 9: Profile for -55°C to 125°C thermal cycling

Post ATC Evaluation and Failure Analysis:
Samples from groups exposed to each of the two ATC profiles were evaluated to determine both the failure modes and to examine the changing microstructure over the course of the test. Samples were selected at time of failure, at the halfway point of each test and at the completion of each test. Each sample was mounted in epoxy, and then ground and polished through the following sequence: 500 and 1200 grade SiC paper, polishing with 6 µm and 1 µm DiaPro diamond suspensions (Struers), and an oxide polish (Struers' OP-S). Optical microscopy was performed using a Nikon Measurescope MM-11. Prior to SEM analysis, the samples were carbon coated using an Emitech K950X. SEM microscopy was performed using a Hitachi S-4500 and Hitachi S-3000N with Oxford and ThermoScientific EDX systems respectively.

RESULTS
Reliability and Failure Analysis Results:
Using IPC-9701A as a guideline, this test focuses on solder joint reliability; other modes of failure, for example those attributed to the laminate material, were removed from consideration in the reliability calculations. Therefore any identified failures that were removed from the test prior to completion and later found to be attributed to something other than solder joint fatigue should be identified as

"censored". Finally, testing was suspended after a predetermined amount of time whether or not failures were identified. Parts that did not fail were identified as "censored". This type of data censoring is referred to as Type 1, or time censored data in which a test is concluded after a predetermined amount of time, in spite of the fact that failures may not have occurred.[23]

0 ℃ to 100 ℃ Accelerated Thermal Cycling

A total of 6010 cycles of ATC from 0-100°C were completed. The test was periodically stopped and the failures, which have been recorded using a data logger, were removed and verified by manual resistance measurement. If the failure was determined to be within the test vehicle, as opposed to a cabling issue, the component was cut out of the board for future failure analysis. The remaining components on the test vehicle where returned to the chamber and the testing continued. Because no failures had been identified at the halfway point of the test, four boards, one for each alloy, were removed for metallurgical analysis. This occurred after 3157 cycles had been completed. These components were identified as "censored".

Table 7 summarizes the number of cycles to first failure of the QFP176s monitored during the 6010 cycles of the test. There are not enough failures at the end of 6010 cycles to plot failure distribution charts for each alloy. Only SAC305 experienced failures when built on High T_g (170°C) board material and those occurred towards the end of the test. Figure 10 shows the distribution of failures of solder joints built on High T_g boards compared with those built on Normal T_g boards. A two-parameter Weibull distribution is used.

The shape parameter determines the shape of the probability distribution and can be viewed by plotting the probability density function (PDF). At values between 3 and 4, the shape parameter approximates a normal distribution. Shape parameter values higher than 4, as shown in Figure 11 results in a near-normal distribution with a left tail. The scale parameter (or slope on the Weibull distribution) described the range of the distribution, or the rate of at which the failure rate increases. It can be seen that the High T_g boards are expected to survive much longer than those built with Normal T_g when using SAC305 as the solder paste.

Table 7: Summary of QFP failures after 0°C-100°C ATC

Component type	High T_g				Normal T_g			
	SAC305	Senju M42	Sunrise	Sunflower	SAC305	Senju M42	Sunrise	Sunflower
QFP176	*2/6*	*0/10*	*0/7*	*0/8*	*6/6*	*0/10*	*1/12*	*0/10*
	33.3%	--	--	--	*100%*	--	*8.3%*	--
Failure Cycle	5792				3534		5416	
	5994				4349			
					4653			
					4782			
					5223			
					5251			

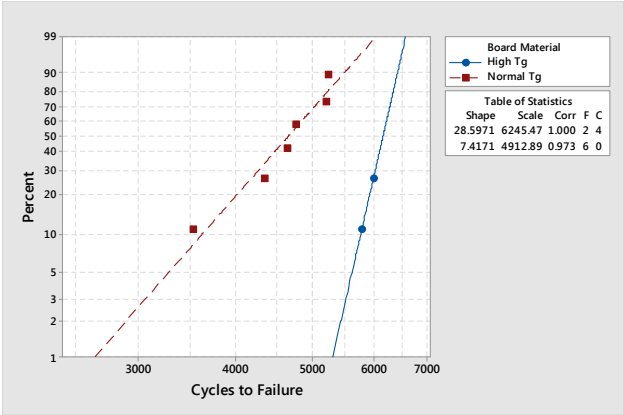

Figure 10: Weibull plots of SAC305 QFP solder joints after 6010 Cycles 0-100°C, High to Normal T_g boards

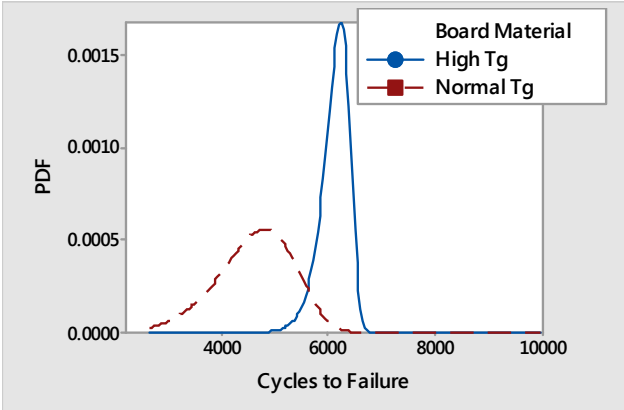

Figure 11: PDF of SAC305 QFP solder joints after 6010 Cycles 0-100°C, High to Normal T_g boards

Figure 12 shows the failure occurred as a result of fracture initiating in the bulk solder and propagating along the lead side IMC layer. This is further illustrated in Figure 13 which shows the fracture surface of a similar solder joint made up of SAC305 on High T_g board material. The area highlighted in red shows the crack initiation. The area highlighted in green illustrates the point at which the fracture moves along the IMC layer. Within the green area, EDX scans were taken of area 1, which was shown to be pure Sn indicating bulk solder and area 2: which was shown to be Cu_6Sn_5 indicating the IMC layer. Finally, the area highlighted in blue shows a ductile fracture, which likely occurred as a result of overload on the remaining area.

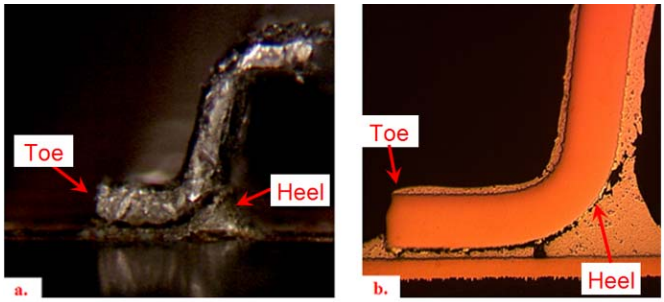

Figure 12: QFP fracture of SAC305 on High T_g board a) optically and b) cross section

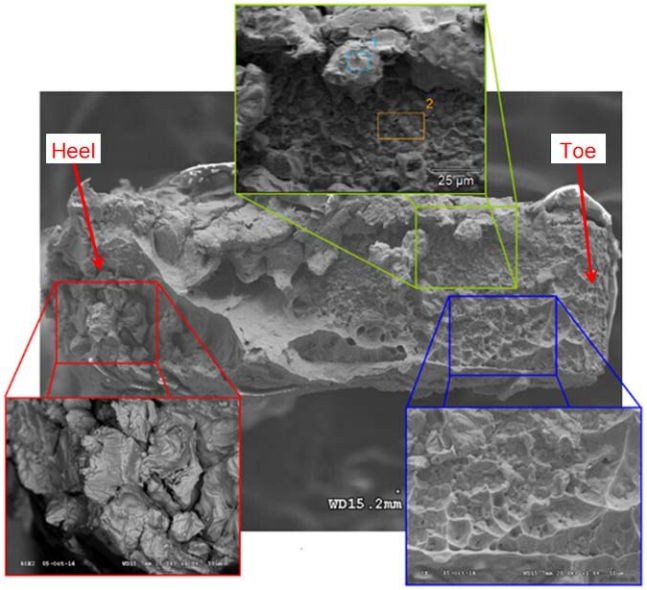

Figure 13: Fracture surface of QFP solder joint with SAC305 on High T_g board after 6010 cycles

Figure 14 shows that fractures had initiated in solder joints formed with the other three alloys on high T_g board material, but by 6010 cycles had not yet propagated far enough into the solder joint to cause an electrical failure. It is expected that these solder joints would ultimately fail in the same manner as shown in Figure 12 and Figure 13 if the testing had continued.

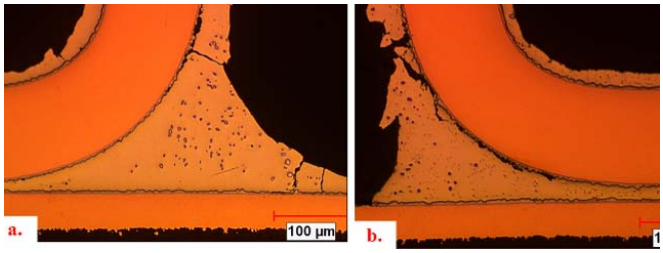

Figure 14: Fracture initiation in QFP a) Sunflower b) Senju M42 after 6010 cycles

The BGA solder joints were made up of paste from the experimental alloy and SAC305 solder balls. This resulted in a solder joint composition closer to SAC305 and with no more than 0.9wt% Bi. No failures occurred within the 6010 cycles of the test when high T_g board material was used. A number of failures occurred for each of the paste alloys when normal T_g board material was used as outlined in Table 8. Using resistance probing, these were all found to be the result of failure within the component-solder-board system; either in the board circuit pattern beneath the component, the solder connecting the component to the board or within the component itself. It is not possible to determine where within this system the failure occurred without destructive techniques. Each component was therefore cut from the board and cross-sectioned to find the point of failure.

Table 8: BGA failures after 0°C-100°C ATC

Component type	Normal T_g			
	SAC305	Senju M42	Sunrise	Sunflower
Fraction failed components	***5/6***	***9/10***	***8/12***	***6/10***
% failed components	***83.3%***	***90.0%***	***66.7%***	***60.0%***
Cycles to Failure	4168	4079	4534	3623
	4612	4540	4619	3930
	5168	4629	4725	4607
	5168	4680	4855	4902
	5278	4861	5153	5086
		5497	5452	5169
		5674	5455	
		5679	5536	
		5871		

Figure 15 illustrates that there is no significant difference in the reliability performance of the solder joints formed using paste of the four alloys on Normal T_g boards. All BGA failures were found to result from board failures, specifically via cracks within the laminate material. The probability distributions for each alloy in this test exhibit similar shape and scale parameters, which is to be expected since all failures are characteristics of the board material and construction, rather than the solder alloy.

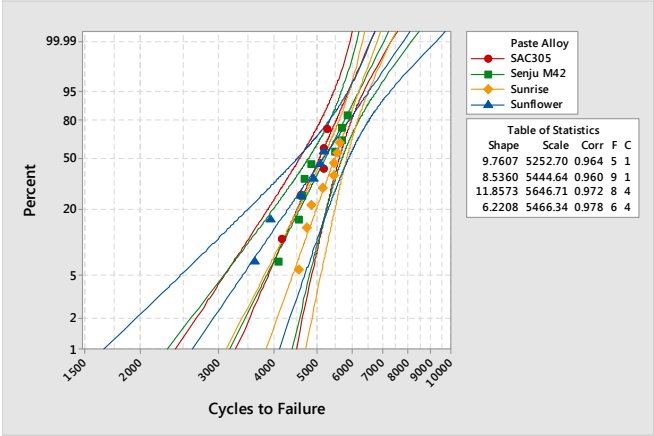

Figure 15: Weibull plots of BGA solder joints on Normal T_g boards after 6010 Cycles 0 to 100°C cycles

Figure 16 illustrates a) a typical via barrel failure and b) a bulk solder fracture – although incomplete failure – near the component side IMC.

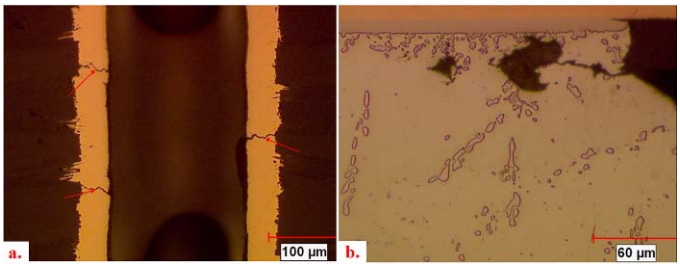

Figure 16: BGA failures after 0 to 100°C ATC a) failure in board material by via plating crack and b) partial failure through bulk solder (SAC305) near component side IMC

-55 ℃ to 125 ℃ Accelerated Thermal Cycling:

A total of 1000 cycles of ATC from -55°C to 125°C, or Harsh Environment ATC, were completed. The test was periodically stopped and the failures, recorded using a data logger, were removed and verified by manual resistance measurement. If, during the course of testing, the failure was determined to be within the test vehicle, as opposed to a cabling issue, the component was cut out of the board for future failure analysis. The remaining components on the test vehicle were returned to the chamber and the testing continued. Four boards, one for each alloy, were removed for metallurgical analysis near the halfway point of the test, after 438 cycles completed. Table 9 summarizes the number of cycles to first failure of the QFP176s monitored during the 1000 cycles of the test.

Table 9: QFP failures after -55°C- 125°C ATC

Component type	High T_g				Normal T_g			
	SAC305	Senju M42	Sunrise	Sunflower	SAC305	Senju M42	Sunrise	Sunflower
failed components	***3/4***	***6/10***	***4/9***	***4/10***	***4/5***	***6/8***	***10/12***	***5/10***
% failed components	***75.0%***	***60.0%***	***44.4%***	***40.0%***	***80.0%***	***75.0%***	***83.3%***	***50.0%***
Cycles to Failure	457	406	81	493	304	428	83	23
	514	446	212	689	544	439	83	480
	820	485	526	897	721	561	285	662
		535	595	909	918	637	459	697
		621				643	528	783
		634				680	601	
							726	
							744	
							843	
							924	

Figure 17 and Figure 18 show probability distribution plots and the probability density functions of the four alloys on High T_g board materials respectively. Sunrise showed some early fails, resulting in a different shape of the PDF. Figure 19 shows probability distribution plots of the four alloys on Normal T_g board materials respectively. In all cases, the distribution of failures occurred within overlapping confidence intervals; there is insufficient data to distinguish between the alloys after 1000 cycles of testing on Normal T_g boards.

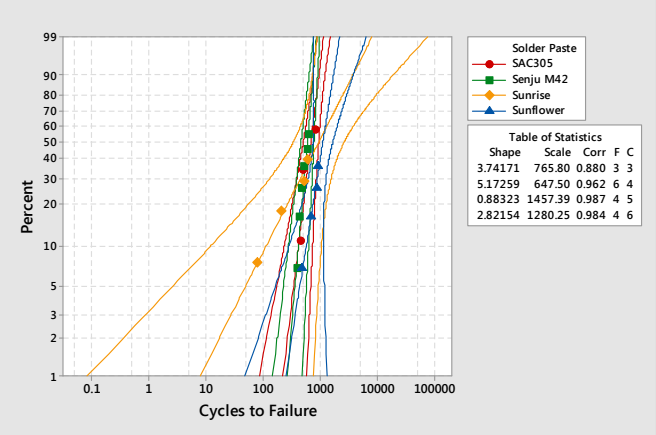

Figure 17: Weibull plots of QFP failures on High T_g boards after 1000 cycles -55 -125°C

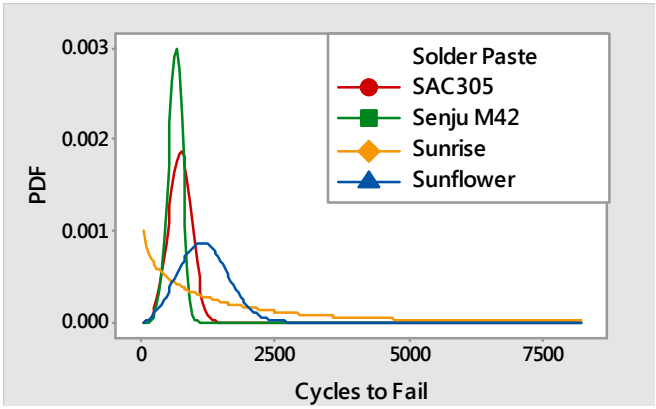

Figure 18: Probability Density Function for QFP failures on High T_g boards after 1000 cycles -55 -125°C

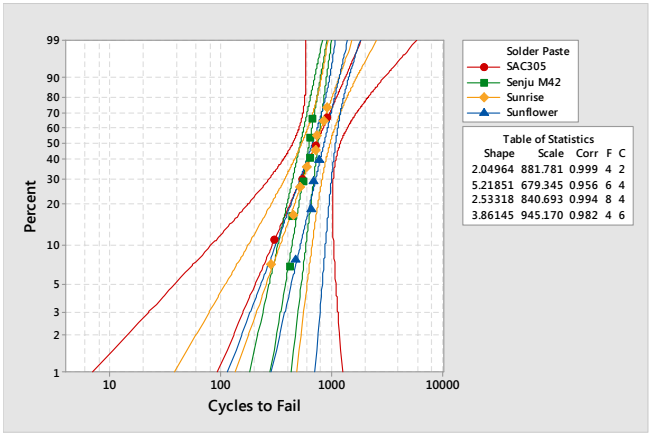

Figure 19: Weibull plots of QFP failures on Normal T_g boards after 1000 Cycles -55-125°C

Just as in the 0 to 100°C cycling test, all QFPs experienced solder fracture initiating in the bulk solder and propagating along the lead side IMC (Figure 20). These however did not result in complete fracture, and would not account for the electrical failure. Further testing, by probing various test points in the test vehicle, determined that the likely cause of electrical failure was the copper trace separating from the board material. Copper trace fractures result in electrical open circuits.

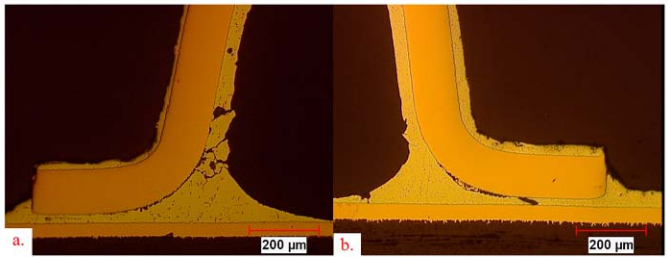

Figure 20: QFP176 fractures in a) Sunflower and b) Senju M42 after 1000 cycles Harsh testing

The BGA components that underwent harsh thermal cycling experienced many failures (Table 10). Upon cross sectional failure analysis however, these failures were found to be the result of board damage, as in the 0-100°C test, specifically

via cracks within the laminate material (Figure 21). While there are enough data points to plot probability distributions, this did not provide a means of distinguishing between alloys.

Table 10: BGA failures after -55°C-125°C ATC

Component type	High T_g				Normal T_g			
	SAC305	Senju M42	Sunrise	Sunflower	SAC305	Senju M42	Sunrise	Sunflower
Failed components	*5/6*	*10/10*	*6/6*	*9/10*	*4/6*	*10/10*	*12/12*	*10/10*
% failed components	*83.3%*	*100.0%*	*100.0%*	*90.0%*	*66.7%*	*100.0 %*	*100.0%*	*100.0%*
Cycles to Failure	407	702	376	522	498	387	325	425
	449	757	518	575	581	459	425	469
	455	772	537	670	615	461	443	561
	815	783	757	692	655	464	447	600
	847	783	783	693		541	467	643
		798	823	696		552	471	672
		878		864		570	491	705
		924		968		597	494	804
		985		999		600	575	837
		999				696	587	934
							848	
							897	

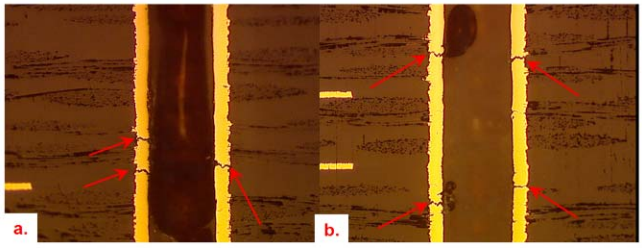

Figure 21: BGA failures after -55 to 125°C ATC failures in board material by via plating crack in boards built with Sunrise and b) boards built with Sunflower

Further examination of the solder joints revealed some crack initiation in the solder joints towards the component side of the BGA solder joint. These crack initiation sites (

Figure 22) were less significant than the damage observed after 6010 cycles of 0-100°C thermal cycling and would not account for a failure reading. Electrical failures, just as in the case of 0-100°C thermal cycling, occurred as a result of via cracks in the board material (Figure 21). A probability plot comparing all failures on the two different board materials (Figure 23) illustrates that the board material was a more significant distinguishing factor than the various solder alloys.

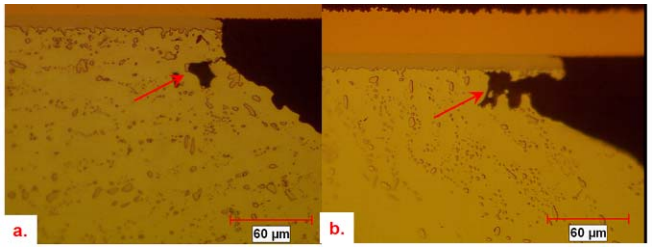

Figure 22: BGA solder crack initiation after -55 to 125°C ATC in solder joints formed with SAC305 solder balls and a) Sunflower and b) Sunrise

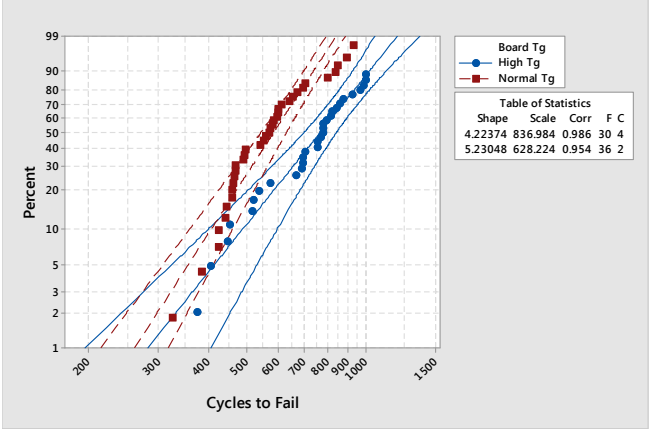

Figure 23: Weibull plots of BGA solder joints after 1000 Cycles -55 to 125C cycles comparing two board materials

QFP solder joint failures on Normal T_g board material was used to compare the two test conditions, 0-100°C for 6010 cycles and -55 to 125°C for 1000 cycles. The Harsh environment test (-55 to 125°C) produced many failures over the 1000 cycles, including a few early failures. This resulted in a Weibull distribution with a shape parameter of 1.26, a PDF with a right tail. The 0-100°C was less severe and therefore resulted in fewer failures and no early failures. The shape parameter of 5.59 indicates that the failure rate increases over time.

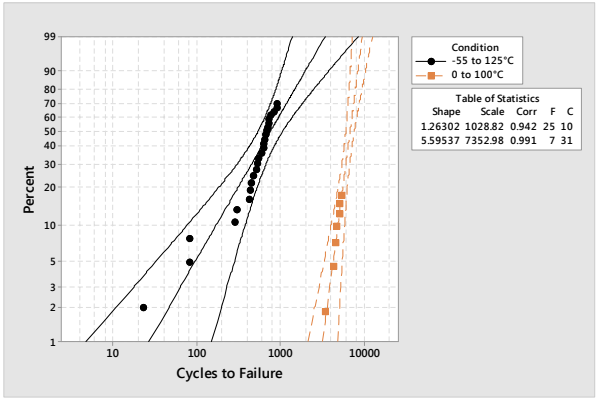

Figure 24: Weibull plot for QFP solder joints on Normal Tg boards comparing two test conditions

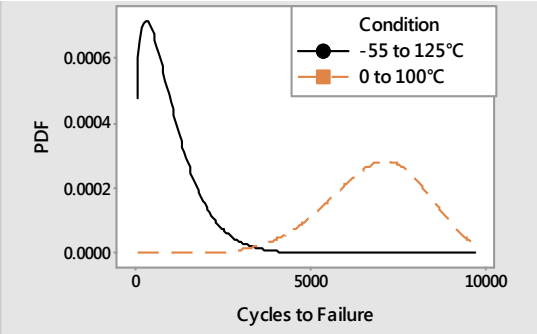

Figure 25: Probability Density Function for QFP failures on Normal Tg boards comparing two test conditions

Microstructure Evaluation

Bulk Microstructure

SAC305, before thermal cycling (Figure 26a and 73b) appears as small dendrite arms surrounded by small Ag_3Sn and Cu_6Sn_5 particles. After thermal cycling from 0 to 100°C for 3148 and 6010 cycles (Figure 26c and 73d respectively) the intermetallic particles coalesced into fewer, larger particles. Senju M42 behaved in the same manner. In both cases, the bulk of the microstructural transition occurred between 0 and 3148 cycles, with little change between 3148 and 6010 cycles. With 3% Bi in Senju M42, there does not appear to be any significant Bi precipitation from the solid solution (Figure 27).

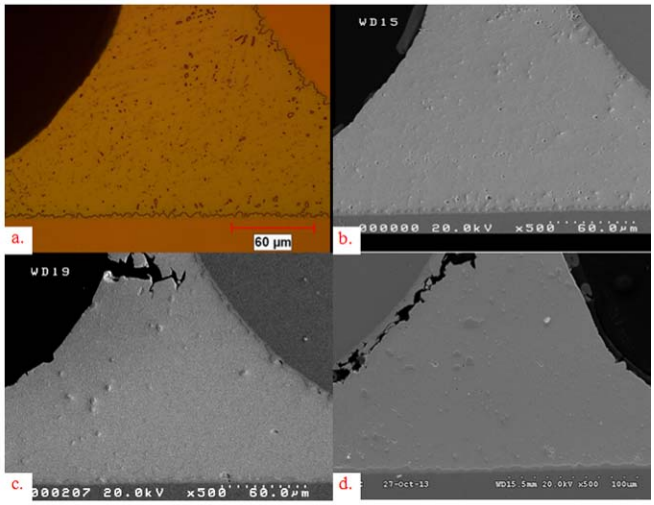

Figure 26: SAC305 at Time 0 a) optically and b) SEM image and after b) 3148 cycles and d) 6010 cycles of 0-100°C ATC

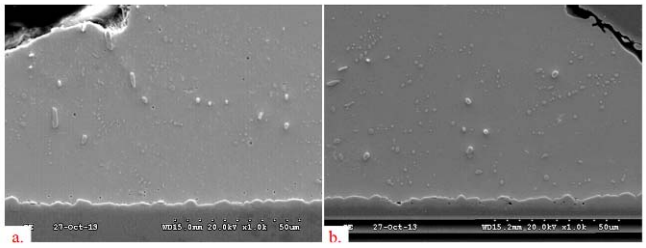

Figure 27: Senju M42 at 1000x after a) 3148 cycles and b) 6010 cycles

Sunrise and Sunflower solder paste alloys, which both contain 7wt% Bi, showed a significant amount of Bi precipitation after ATC. In both cases large, uneven particles of Bi were present upon solidification, as seen in Chapter 2. After ATC, Sunrise showed many, very small particles precipitated throughout the bulk, evenly dispersed from the βSn grains (Figure 28). Sunflower also exhibited some Bi accumulation along the grain boundaries (Figure 29). In both cases, there did not appear to be any significant accumulation of Bi along the interface with the interfacial IMC layer.

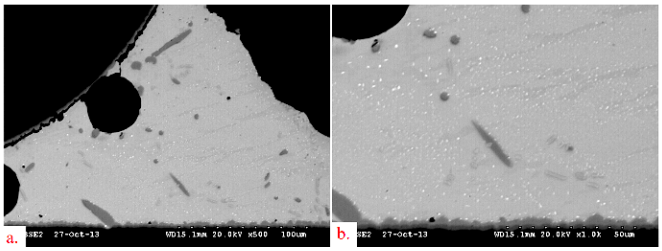

Figure 28: Sunrise after 6010 cycles 0-100°C at a) 500x and b) 1000x

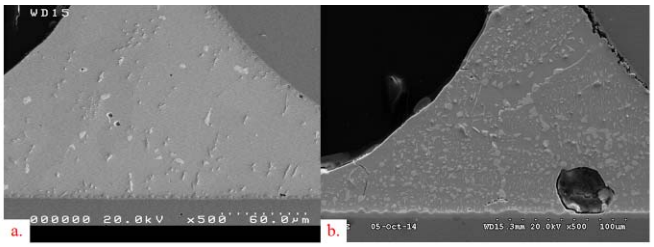

Figure 29: Sunflower at a) Time 0 and b) after 6010 cycles 0-100°C at 500x

IMC Growth during Thermal Cycling

The interfacial IMC layers were measured at 30 to 45 locations for each component. A comparison of the board side IMC layer of a QFP176 component follows. This IMC layer formed during the reflow process in which a bond was formed between the board side copper pad and the molten solder. The Time 0 results reference this IMC layer after reflow but before any thermal cycling. Only Cu_6Sn_5 was identified at Time 0. Measurements were made after approximately the halfway point and again at the completion of the two thermal cycling regimes. For the 0-100°C test, measurements were completed after 3157 cycles and then again after 6010 cycles. For the harsh environment test (-55°C to 125°C) measurements were taken at 438 cycles and then again at 1000 cycles. After exposure to thermal cycling, both Cu_6Sn_5 and Cu_3Sn species were identified (Figure 30).

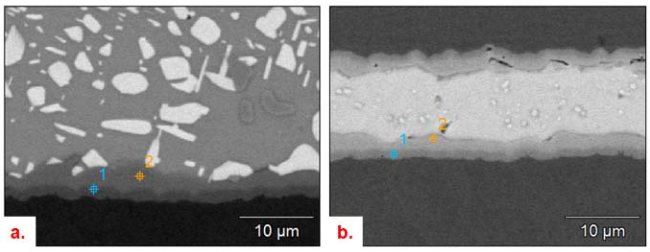

Figure 30: IMC layers formed on QFP176 solder joints between the board side Cu layer and solder paste a) sunrise and b) SAC305 after 438 cycles of Harsh thermal cycling. Location 1 shows the Cu_3Sn layer, location 2 shows the Cu_6Sn_5 layer

Figure 31 provides a comparison of the overall IMC thickness at the various test intervals; Figure 32 provides a comparison of the Cu_3Sn layer within the IMC at various test intervals. Table 11 and

Table 12 provide a summary of results from two-sided T-test to compare the mean values and Levine-test to compare the variance of the IMC and Cu_3Sn thicknesses respectively. These tables are provided in order to examine the changes in thickness of the overall IMC and the Cu_3Sn layers, for each alloy, over the course of the two thermal cycling conditions. The tables provide probability (p-values) for each test. In all cases, the null and alternate hypotheses are as follows:

$$H_0: \mu_1=\mu_2 \textbf{ and } \sigma_1=\sigma_2$$

$$H_a: \mu_1\neq\mu_2 \textbf{ and } \sigma_1\neq\sigma_2$$

Values in Table 11 and

Table 12 which are ***bold italicized*** represent points with a p-value less than 0.05. This indicates that H_0 should be rejected at a 95% confidence level and the H_a is assumed to be valid. In this case, it assumes that the mean value has changed. These results show that between 0 and 1000 cycles of Harsh testing, the IMC layers for each alloy increased significantly. For Senju M42 and Sunrise, this occurred primarily within the first 438 cycles. For SAC305 and Sunflower the increase continued throughout the test. In 0-100°C ATC testing, the IMC layer for all alloys except SAC305 increased throughout the test. The IMC thickness for SAC305 increased most significantly during the first half of the test. All t-tests of the µ in

Table 12 result in rejecting the H_0. This indicates that the thickness of the Cu_3Sn layer continues to increase throughout the course of the two tests. Table 13 provides a summary of test for equal variance and ANOVA testing of the various alloys. This test compares the IMC and Cu_3Sn thicknesses of all four alloys, at a given point during ATC. This table provides probability for each test. In all cases, the null and alternate hypotheses are as follows:

$$H_0: \mu_{SAC305}=\mu_{Senju\ M42}=\mu_{Sunrise}=\mu_{Sunflower} \text{ and } \sigma_{SAC305}=\sigma_{Senju\ M42}=\sigma_{Sunrise}=\sigma_{Sunflower}$$

H_a: at least one µ is different and at least one σ is different

The result of ANOVA testing, indicated in Table 13: ANOVA test equal variance and means, show that while the total IMC thickness increased relatively consistently among the four alloys, the increase in the thickness of the Cu_3Sn layer was different in at least one alloy. Figure 32 clearly shows that Sunflower exhibited a significantly thicker Cu_3Sn layer after Time 0 in both test conditions.

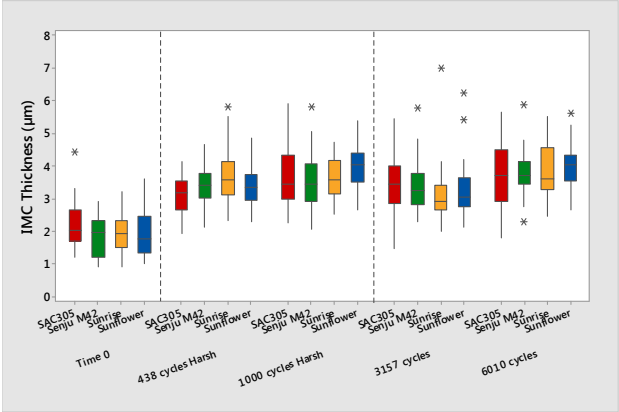

Figure 31: IMC growth at the board side of QFP during thermal cycling

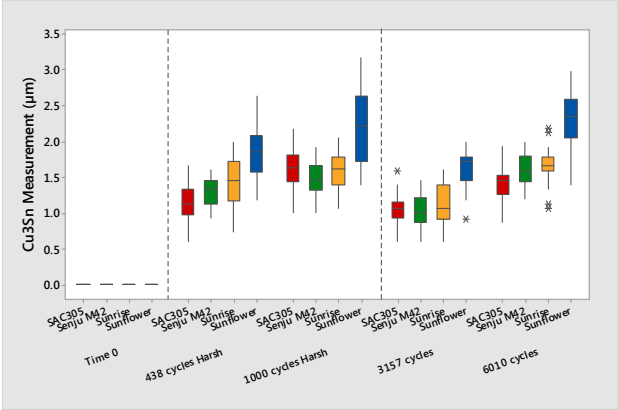

Figure 32: Cu_3Sn (portion of IMC) growth at board side of QFP during thermal cycling

Table 11: Results of Levine-Test to compare the variance (σ) of IMC measurement and 2-sided t-Test to compare the means (μ) of IMC measurements

Test Condition	HARSH (-55 to 125°C)						(0 to 100°C)					
Comparison	0 to 438 cycles		0 to 1000 cycles		438 -1000 cycles		0 to 3157 cycles		0 to 6010 cycles		3157 - 6010 cycles	
Variable / p value	σ	μ	σ		σ	μ	σ	μ	σ	μ	σ	μ
SAC305	0.40	***0.00***	0.21	***0.00***	***0.04***	***0.03***	0.23	***0.00***	0.11	***0.00***	0.74	0.56
Senju M42	0.72	***0.00***	0.17	***0.00***	0.11	0.49	0.53	***0.00***	0.97	***0.00***	0.61	***0.04***
Sunrise	***0.03***	***0.00***	0.13	***0.00***	0.43	0.85	0.53	***0.00***	0.02	***0.00***	0.40	***0.00***
Sunflower	0.28	***0.00***	0.75	***0.00***	0.26	***0.00***	0.31	***0.00***	0.87	***0.00***	0.39	***0.00***

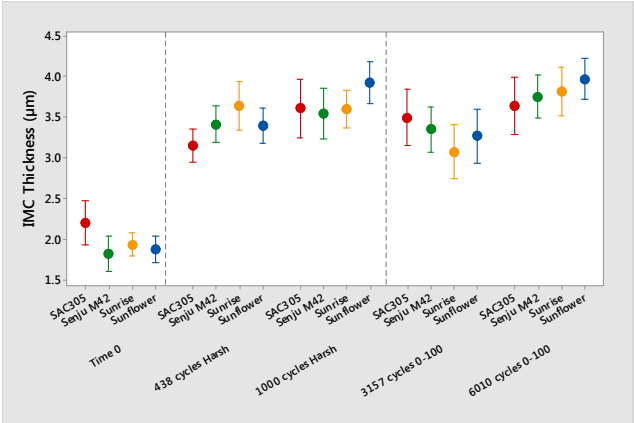

Figure 33: Interval plot of IMC thickness

Table 12: Results of Levine-Test to compare the variance (σ) of Cu_3Sn measurement and 2-sided t-Test to compare the means (μ) of Cu_3Sn measurements

Test Condition	HARSH (-55 to 125°C)		(0 to 100°C)	
Comparison	438 to 1000 cycles		3157 to 6010 cycles	
variable	σ	μ	σ	μ
SAC305	0.40	***0.00***	0.72	***0.00***
Senju M42	0.70	***0.00***	0.99	***0.00***
Sunrise	0.17	***0.04***	0.17	***0.00***
Sunflower	***0.01***	***0.00***	***0.04***	***0.00***

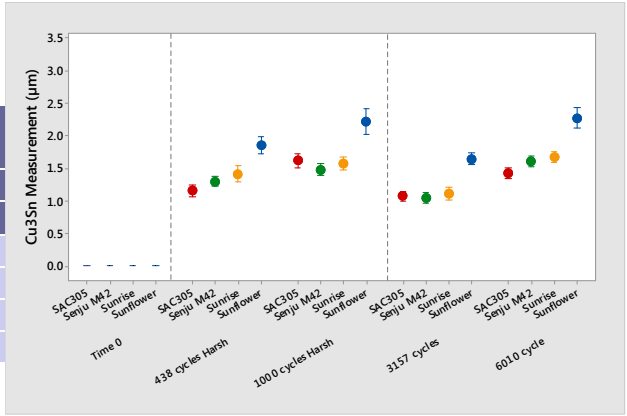

Figure 34: Interval plot of Cu_3Sn thickness

Table 13: ANOVA test equal variance and means

Variable / p value		Total IMC		Cu_3Sn	
		Eq var (σ)	ANOVA (μ)	Eq var (σ)	ANOVA (μ)
Test Condition	Time 0	0.60	0.07	--	--
	438 cycles (-55 to 125°C)	0.20	***0.04***	***0.01***	***0.00***
	1000 cycles (-55 to 125°C)	0.35	0.24	***0.00***	***0.00***
	3157 cycles (0 to 100°C)	0.65	0.30	0.56	***0.00***
	6010 cycles (0 to 100°C)	0.13	0.43	***0.01***	***0.00***

Figure 33 through Figure 40 provide details of the ANOVA analysis. The interval plot Figure 33 and Figure 34 show the 95% confidence intervals for the mean overall IMC layer thickness and the mean Cu_3Sn layer thickness respectively. While it appears that SAC305 has a thicker overall IMC layer at Time 0, the interval plot shows substantial overlap between the 95% CIs of all four alloys and therefore indicates that the difference in thickness is not statistically significant. Further analysis indicates that there is a difference in Time 0 thicknesses within a 93% confidence level. The thicker IMC layer of SAC305 is a result of the higher processing temperature (240°C). The intervals for the Cu_3Sn layer thickness of Sunflower do not overlap with any of the 95% CI of the other alloys, thereby indicating a significant difference in thickness.

The main effects plots in Figure 35 to Figure 38 are used to de-couple the main factors in the measurements to better understand their individual contributions. Figure 35 and Figure 36 show the condition, or time at exposure to thermal cycling, has a greater influence on the overall IMC thickness than do the particular alloys. SAC305 has a Time 0 IMC thickness greater than the mean of the other three alloys, which all have mean values closer to the grand mean. Figure 37 and Figure 38 show that the condition is also a greater influence on the mean overall thickness of the mean Cu_3Sn layer than the alloys. The difference between Cu_3Sn thicknesses amongst the alloys shows the same pattern: SAC305 and Senju M42 have mean thicknesses close to the grand mean, Sunrise has a mean lower than the grand mean and Sunflower is significantly greater than the grand mean.

Figure 35: Main effects plot of IMC thickness at the board side QFP during HARSH (-55 to 125°C) ATC

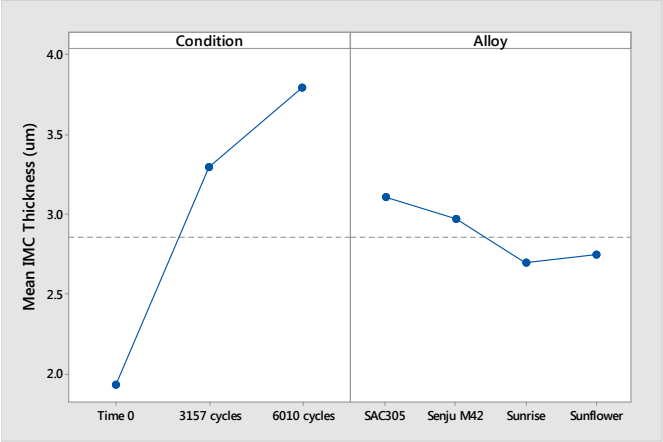

Figure 36: Main effects plot of IMC thickness at the board side QFP during 0-100°C

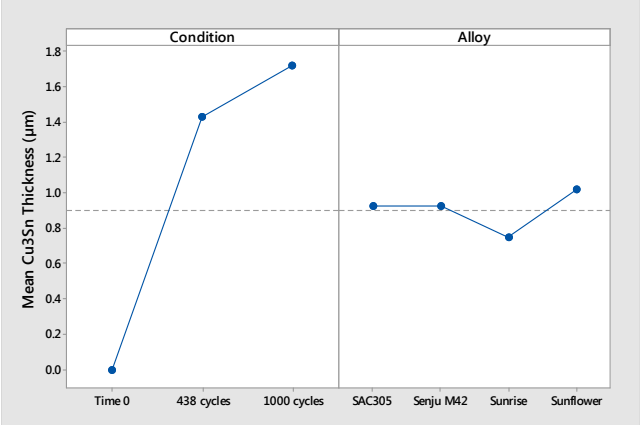

Figure 37: Main effects plot of Cu_3Sn thickness at board side of QFP during HARSH (-55 to 125°C) ATC

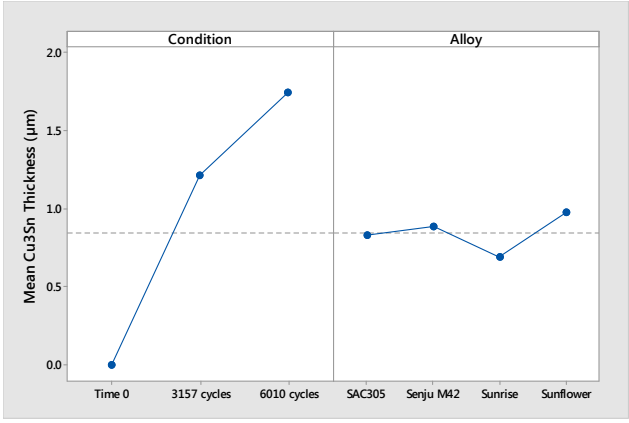

Figure 38: Main effects plot of Cu_3Sn thickness board side of QFP during 0-100°C

Interaction plots found in Figure 39 and Figure 40 tests the factors to identify any interactions. Parallel, or near parallel lines, as seen in both cases indicate there are no clear interactions; the influence of one factor is not dependent on the other. The mean thickness of the IMC layer for SAC305 at Time 0 is greater than that of the other alloys, however over the course of ACT testing under two test conditions, this distinction seems to disappear, the mean IMC thicknesses are no longer distinguishable between alloys.

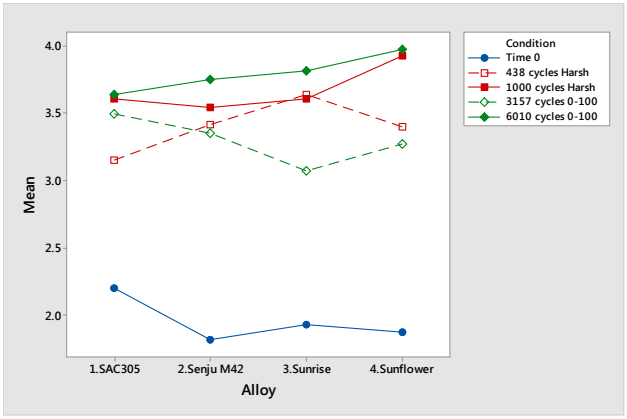

Figure 39: Interaction plot of IMC thickness at the board side of QFP after ATC

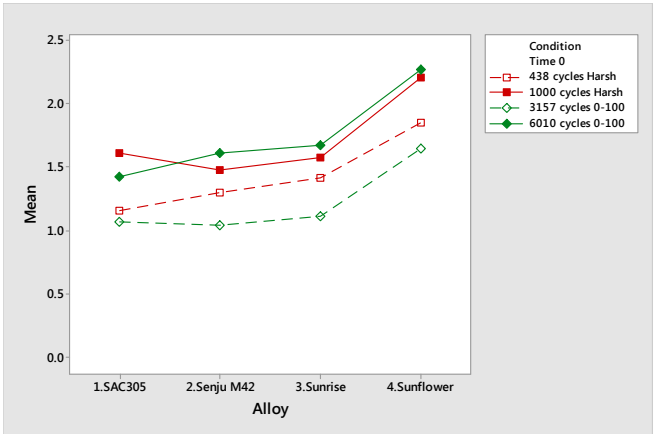

Figure 40: Interaction Plot of Cu_3Sn Thickness at Board Side of QFP after ATC

SUMMARY OF FINDINGS AND CONCLUSIONS

Findings Based on Reliability Data

During two different thermal cycling regimes the only failures which could be attributed to solder joint fatigue failures occurred in SAC305 during 0 to 100°C cycling; one sample of Sunrise, which failed but only after 5416 cycles. All other electrical failures were attributed to failures within the board material. In the case of BGAs, this occurred due to cracks within via barrels; in QFPs it was the result of copper trace fractures. Thermal cycling did not significantly distinguish between the reliability performances of the four alloys. High T_g board material appeared to outperform Normal T_g board material. It can be concluded that the three lower process temperature solders performed as well as, or better than SAC305 during accelerate thermal cycling. All solders survived longer than the board materials.

Findings Based on Microstructural Observations

Bi had a beneficial impact on the bulk microstructure. It precipitated from the bulk solder evenly in very small particles. This favorable influence of Bi only appeared when the concentration was 7wt%; the 3wt% Bi of Senju M42 did not appear to have the same impact. Senju M42 appeared to have the same aging characteristics as SAC305. There was some degree of Bi segregation along the grain boundary observed in the Sunflower alloy; however there did not appear to be full segregation of the phases.

The interfacial IMC layer (η) Cu_6Sn_5, formed during solidification, was similar in thickness for all alloys. During thermal cycling, the total thickness of the interfacial IMC continued to increase, as well as (ε) Cu_3Sn layer formation. While the overall thickness increased similarly for all four alloys, the Cu_3Sn layer of the Sunflower alloy was much thicker than the other alloys. This alloy has no Ag, which indicates that Ag plays a role in suppressing Cu_3Sn growth. This is in spite of the fact that Ag does not participate in the IMC formation; no Ag-containing species exists at the interfacial IMC. It has previously been shown that eutectic SnAg solder exhibited a lower layer-growth coefficient for Cu_6Sn_5 than for Cu_3Sn.[24] This was believed to be the result of the Sn diffusion in SnAg being slower than the Sn diffusion in, for example eutectic SnPb solder, in turn favoring the growth of Cu_3Sn. It appears, through this study, that even small amounts of Ag in the solder (1%, 2% and 3%) are sufficient to suppress the diffusion of Sn to the growing interfacial IMC layers. Bi alloying did not significantly change the growth rates of either intermetallic compound. The increased growth of the Cu_3Sn phase in the Sunflower alloy did not correspond to any decrease in reliability during ATC.

SAC305, which was processed at a higher temperature, initially had a larger interfacial IMC layer. This effect however did not continue during thermal cycling where the IMC layers of all four alloys formed and increased to similar overall thicknesses.

REFERENCES

[1] J. Bentley "Introduction to Reliability and Quality Engineering", 2nd Ed, Essex, England, Pearson Education Limited, 1999, ch. 2, pp 28-43.

[2] IPC-SM-785 Guidelines for Accelerated Reliability Testing of Surface Mount Solder Attachments, November 1992

[3] W. Engelmaier "Solder Attachment Reliability, Accelerated Testing, and Results Evaluation" in *Solder Joint Reliability* J.H. Lau, Ed. New York, Springer 1991, ch.17. pp. 545-587

[4] Blueprints for Product Reliability, The Reliability Information Analysis Center (RIAC), http://theriac.org/DeskReference/viewDocument.php?id=280&Scope=blueprints&Deskref=blueprint1#3point4

[5] J.W.Evans "Thermomechanical Fatigue" in *A Guide to Lead-free Solder: Physical Metallurgy and Reliability*, W. Engelmaier, Ed. London, UK, Springer 2007, ch.7, pp. 145-185

[6] IPC-9701A: Performance Test Methods and Qualification Requirements for Surface Mount Solder Attachments, February 2006

[7] A. MacDiarmid "Thermal Cycling Failure – Part One of Two" in The Journal of the Reliability Information Analysis Center, January 2011

[8] J-P.M. Clech and J.A. Augis "Surface Mount Attachment Reliability and Figures of Merit for Design for Reliability in *Solder Joint Reliability* J.H. Lau, Ed. New York, Springer 1991, ch.18. pp. 588-613

[9] J.W.Evans "Introduction to Solder Alloys and Their Properties" in *A Guide to Lead-free Solder: Physical Metallurgy and Reliability*, Ed. London, UK, Springer 2007, ch.1, pp. 1-27

[10] A. Zbrzezny "Characterization and Modeling of Microstructural Evolution of Near-Eutectic Sn-Ag-Cu Solder Joints" Ph.D. Thesis, Dept. MSE, Univ. Toronto, Toronto, Canada, 2004.

[11] R. Coyle, R. Parker, M. Osterman, S. Longgood, K. Sweatman, E. Benedetto, A. Allen, E. George, J. Smetana, K. Howell, J. Arnold "iNemi Pb-Free Alloy Characterization Project Report: Part V – The Effect of Dwell Time on Thermal Fatigue Reliability" presented at SMTAI, Chicago, Il, 2013

[12] J. Juarez Jr., M. Robinson, J. Heebink, P. Snugovsky, E. Kosiba, J. Kennedy, Z. Bagheri, S. Suthakaran, M. Romansky "Reliability Screening of Lower Melting Point Pb-Free Alloys Containing Bi," in IPC APEX EXPO Conference, Las Vegas, NV, 2014.

[13] B. Arfaei, M. Anselm, S. Joshi, S. Mahin-Shirazi, P. Borgesen, E. Cotts, J. Wilcox, and R. Coyle "Effect of Sn Grain Morphology on Failure Mechanism and Reliability of Lead-Free Solder Joints in Thermal Cycling Tests", presented at SMTAI, Chicago, Il, 2013

[14] K-N. Tu "Copper Tin Reactions in Thin-Film Samples" in *Solder Joint Technology : Materials, Properties*

and Reliability New York, Springer, 2007, ch. 3, pp. 73-108.

[15] N. Mookam and K. Kanlayasiri "Evolution of Intermetallic Compounds between Sn-0.3Ag-0.7Cu Low-Ag Lead-free Solder and Cu Substrate during Thermal Aging" J. Mater. Sci. Technol., 2012, 28(1), 53-59.

[16] C. Yu, Y.Yang, P. Li, J. Chen, H. Lu "Suppression of Cu_3Sn and Kirkendall voids at Cu/Sn-3.5Ag solder joints by adding a small amount of Ge", J.Mater Sci: Mater Electron (2012) 23:56-60

[17] C. Yu Chen, Kai-Yun Wang, Jing-Qing Chen, Hao Lu "Suppression effect of Cu and Ag on Cu_3Sn layer in solder joints", J Mater Sci: Mater Electron (2013) 24:4690-4635

[18] G.C. Moon, S.K. Kang, D-Y Shin and H.M. Lee "Effects of Minor Additions of Zn on Interfacial Reactions of Sn-Ag-Cu and Sn-Cu Solders with Various Cu Substrates during Thermal Aging" Journal of Electronic Materials, Vol. 36, no. 11, 2007.

[19] P. Snugovsky, E. Kosiba, J. Kennedy, Z. Bagheri, M. Romansky, M. Robinson, J.M. Juarez, Jr., J.Heebink "Manufacturability and Reliability Screening of Lower Melting Point Pb-free Alloys Containing Bi," in IPC APEX EXPO Conference, San Deigo, CA, 2013.

[20] P. Vianco, and J.A. Rejent "Properties of Ternary Sn-Ag-Bi Solder Alloys: Part 1 – Thermal Properties and Microstructural Analysis", Journal of Electronic Materials, Vol.28, No.10, pp. 1127-1137, 1999

[21] D.Witkin "Creep Behavior of Bi-Containing Lead-Free Solder Alloys" Journal of Electronic Materials, Vol. 41, No. 2, 2012.

[22] P. Vianco, and J.A. Rejent "Properties of Ternary Sn-Ag-Bi Solder Alloys: Part 1 – Thermal Properties and Microstructural Analysis", Journal of Electronic Materials, Vol.28, No.10, pp. 1127-1137, 1999

[23] CRE Primer, Chapter IX: Data Collection, p. IX-5, Quality Council of Indiana. 2009.

[24] D.Kwon "Intermetallic Formation and Growth" in *A Guide to Lead-free Solders: Physical Metallurgy and Reliability,* Silver Spring, MD: Springer, 2005, pp. 97-126